Nanoconstructs

DOI: 10.1002/anie.200903100

Solvent-Free Protein Liquids and Liquid Crystals**

*Adam W. Perriman, Helmut Cölfen, Roy W. Hughes, Claire L. Barrie, and Stephen Mann**

Nanostructures such as functionalized nanoparticles and superlattices have wide-ranging applications in diverse areas.[1–4] Although these materials are invariably used in the form of aqueous/organic dispersions, ultrathin films, or bulk powders, Giannellis and co-workers have recently pioneered an approach to preparing functionalized inorganic nanostructures with liquidlike behavior.[5,6] These are produced by electrostatically grafting an organic canopy layer onto the surface of charged nanoparticles of silica,[7] iron oxides,[7] and titania[8] for example, to provide a fluidization medium for the preparation of solvent-free nanoparticle ionic fluids. Like nanoscale objects in general, proteins exhibit persistent structures with dimensions that exceed the range of their intermolecular forces, such that liquid–vapor co-existence is unattainable.[9] As a consequence, solid-state proteins sublime at low pressures or thermally degrade under ambient conditions: thus, there are no known liquid proteins in the absence of solvent.

Herein, we report, to our knowledge, the first example of a solvent-free liquid protein. Specifically, we report the preparation and properties of a protein melt based on a stoichiometric ferritin–polymer nanoscale construct with surface modifications that extend the range of intermolecular interactions to a length scale that is commensurate with fluidity in the absence of water. Moreover, we show that these spherically shaped nano-constructs undergo anisotropic ordering during melting at 30 °C to produce a viscoelastic protein liquid that exhibits thermotropic liquid-crystalline behavior, and which subsequently transforms to a Newtonian fluid at temperatures above 40 °C and is stable up to a temperature of 405 °C. The method, which utilizes the site-specificity of surface amino acid residues and high degree of uniformity in ferritin molecular architecture to produce discrete single-component ferritin–polymer constructs (Supporting Information, Figure S1), should be readily accessible to exploitation as a facile route to solvent-free liquid proteins and enzymes in general.

Electrostatically induced complexation of cationized ferritin (**C**-Fn), comprising approximately 240 covalently coupled *N*,*N*-dimethyl-1,3-propanediamine (DMPA) groups per molecule (10 DMPA per subunit; Supporting Information, Figure S2), with the anionic polymer surfactant C_9H_{19}-C_6H_4-$(OCH_2CH_2)_{20}O(CH_2)_3SO_3^-$ (**S**) resulted in the formation of the ionic nanoconstruct [**C**-Fn][**S**]. Sedimentation-coefficient distributions obtained by analytical ultracentrifugation of extensively dialyzed aqueous solutions of [**C**-Fn][**S**] showed a single peak centered at 37 S compared with values of 51 or 0.5 S for **C**-Fn or **S** alone (Supporting Information, Figure S3). The decrease in density of the conjugate compared with non-complexed **C**-Fn, as well as the absence of unbound surfactant, were consistent with a discrete protein–polymer ionic construct. Significantly, calculations based on comparative density variations coupled with changes in molecular radius associated with electrostatic conjugation, gave a [**C**-Fn]:[**S**] stoichiometry of 1:264 (Supporting Information). This was consistent with a persistent surface charge-matched ferritin–polymer nanostructure comprising on average eleven electrostatically coupled polymer chains per cationized subunit and a theoretical polymer content of 34 wt %. Similar experiments and calculations undertaken on conjugates prepared from native ferritin also confirmed the formation of a single component construct but with a [Fn]:[**S**] stoichiometry of 1:96 (i.e. four surfactant molecules per subunit).

Protein melts were prepared in the absence of water by lyophilization of the aqueous [**C**-Fn][**S**] solutions to produce a low-density solid that was subsequently annealed at 50 °C to produce a transparent, viscous, red liquid that remained fluid when cooled to room temperature, but re-solidified at −50 °C (Figure 1). TEM studies of the melt revealed discrete electron-dense nanoparticles, approximately 8 nm in diameter, indicating that the protein nanostructure remained structurally intact in the liquid state (Supporting Information, Figure S4). The melts were readily soluble in water or dichloromethane. Thermogravimetric analysis of the melt gave a water content of less than 2 % and a residual mass at 1200 °C of 13 %, which corresponded to the iron oxide cores of the protein. The melt decomposed at 405 °C, compared with 315 and 380 °C for native ferritin and **S**, respectively, indicating cooperative stabilization and decomposition that were consistent with a stoichiometric complex. Significantly, differential scanning calorimetry (DSC) on annealed samples showed significant changes in the enthalpic phase transitions between **S** and the [**C**-Fn][**S**] ionic nanoconstruct (Figure 2a). For **S**, a large asymmetric endothermic transition consisting of a shoulder at 20 °C and a minimum at 27.5 °C was evident on heating, consistent with a two-stage process involving melting

[*] Dr. A. W. Perriman, Prof. S. Mann
Centre for Organized Matter Chemistry, School of Chemistry
University of Bristol, Bristol BS8 1TS (UK)
E-mail: s.mann@bristol.ac.uk
Dr. R. W. Hughes, Dr. C. L. Barrie
Bristol Colloid Centre, School of Chemistry, University of Bristol
Dr. H. Cölfen
Max-Planck-Institut für Kolloid- und Grenzflächenforschung
Am Mühlenberg, 14476 Golm (Germany)

[**] We thank EPSRC (Platform grant EP/C518748/1) for financial support, John Mitchels for help with AFM studies, Prof. Rob Richardson for assistance with X-ray scattering experiments, and Dr. Charl Faul and Martin Hollamby for useful discussions. Antje Völkel is acknowledged for performing the analytical ultracentrifugation experiments.

Supporting information for this article is available on the WWW under http://dx.doi.org/10.1002/anie.200903100.

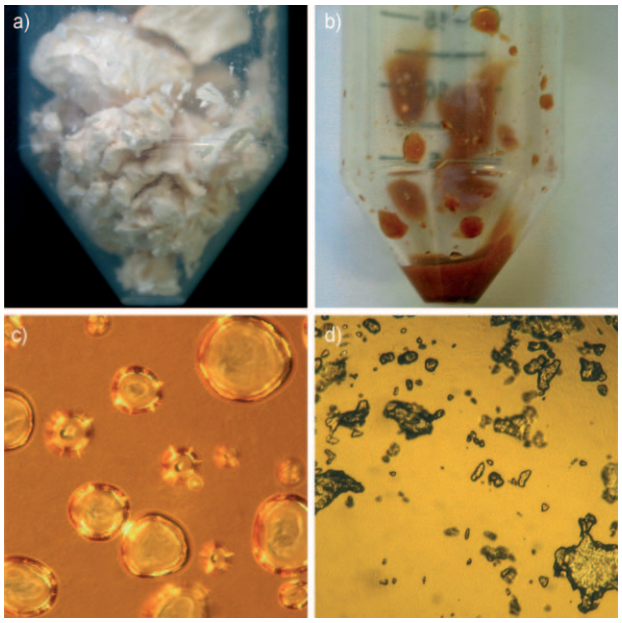

Figure 1. a),b) Lyophilized samples of [**C**-Fn][**S**] constructs, a) before and b) after annealing at 50 °C followed by cooling to room temperature. c),d) Optical microscopy images showing, c) [**C**-Fn][**S**] protein melt at 50 °C, and d) corresponding solid phase at −50 °C. Differences in viscosity are clearly highlighted from changes in the morphology of entrapped air bubbles. Further annealing on the samples resulted in no observable changes in the melt morphology.

of the hydrocarbon and polyethylene oxide chains. A similar melting event was evident at 29 °C for [**C**-Fn][**S**], but was followed by a second discrete endothermic transition at approximately 36.5 °C (Figure 2a, arrow). Upon heating from −50 °C, both **S** and [**C**-Fn][**S**] exhibited an exothermic first-order crystallization phase transition at −14 °C and −18.8 °C, respectively, although only **S** displayed a crystallization peak (at ca. 4 °C) on cooling, which suggested that the ordering processes were kinetically different. Isothermal cycles showed complete reversibility and no thermal hysteresis.

Rheometry was used to study the flow properties of the [**C**-Fn][**S**] melt at temperatures of 32 °C and 50 °C, which were, respectively, between and above the two endothermic transitions observed by DSC. At 50 °C, the [**C**-Fn][**S**] melt exhibited Newtonian fluid behavior with a viscosity of approximately 10 Pa s, consistent with the formation of a liquid protein in the absence of solvent (Figure 2b). In contrast, shear thinning was exhibited by **S** alone, indicative of surfactant–surfactant ordering interactions in the molten state at 50 °C (Figure 2b). Cooling to 32 °C resulted in an increase in viscosity to approximately 20 Pa s at low shear for both samples, with continued Newtonian and non-Newtonian fluid behavior for [**C**-Fn][**S**] and **S** respectively. Significantly, after 16 h at 32 °C, the [**C**-Fn][**S**] melt became more viscous, and showed extensive shear thinning with an abrupt change to a limiting high shear viscosity at a stress of approximately 250 Pa (Figure 2b), which was unrecoverable in simple shear. At 32 °C, these samples showed reproducible frequency sweeps of the storage (G′) and loss (G″) moduli with typical values of 0.8 and 4 Pa, respectively, at a frequency of 1 Hz

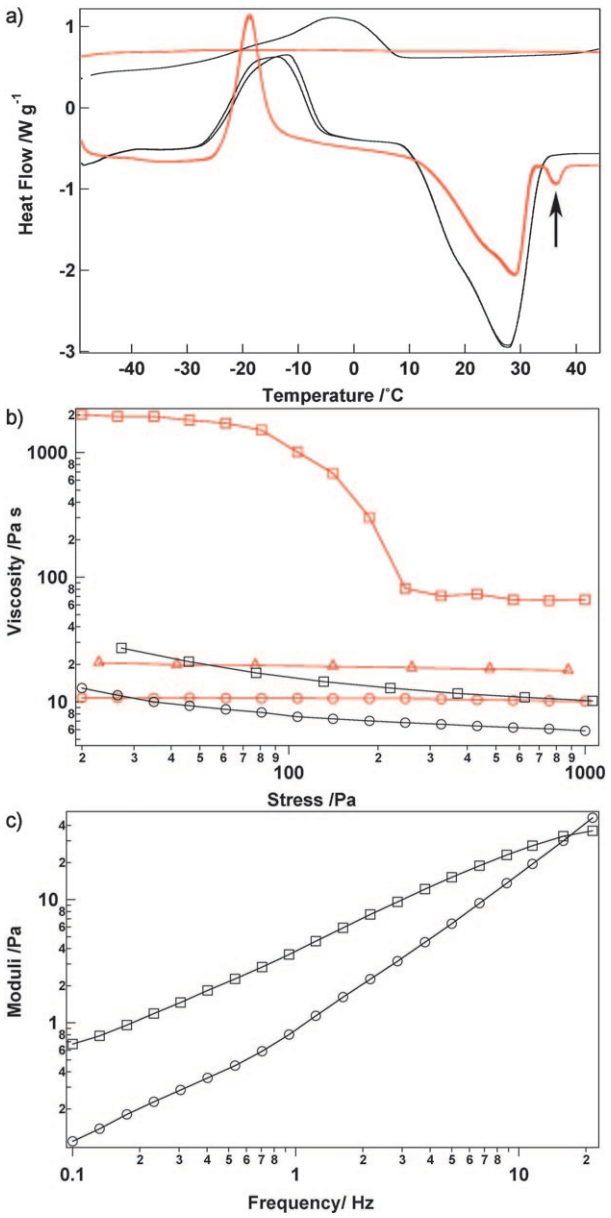

Figure 2. a) DSC traces recorded after one thermal cycle for the anionic polymer surfactant **S** (black line) and the [**C**-Fn][**S**] construct (red line) showing melting transitions with minima at 27.5 and 29 °C, respectively. Samples were annealed at a rate of 10 °C minute^{-1} and isothermal cycles showed complete reversibility and no thermal hysteresis. Arrow indicates a second discrete endothermic transition at approximately 36.5 °C for the [**C**-Fn][**S**] ionic construct. b) Flow curves for [**C**-Fn][**S**] melts at 50 °C (○), after 30 min cooling from 50 to 32 °C (△), and after 16 h cooling from 50 to 32 °C (□). Similar curves for anionic polymer surfactant **S** are shown at 50 °C (○) and at 32 °C (□). c) Storage (G′, ○) and loss (G″, □) moduli of the [**C**-Fn][**S**] melt as a function of frequency at 32 °C after 16 h post-shear.

(Figure 2c). Values of G″ were greater than G′ up to a cross-over frequency equivalent to a relaxation time of approximately 10 ms.

The rheometry results indicated that the [**C**-Fn][**S**] melt underwent a slow ordering transformation at 32 °C from a Newtonian liquid to a viscoelastic liquid that exhibited properties consistent with a liquid-crystalline phase. Signifi-

cantly, [**C**-Fn][**S**] melts subjected to the same temperature program used in the DSC experiments (10 °C min^{-1}) exhibited strong birefringence at 32 °C in the form of a distinct Maltese cross texture when viewed in polarized light (Figure 3a). This

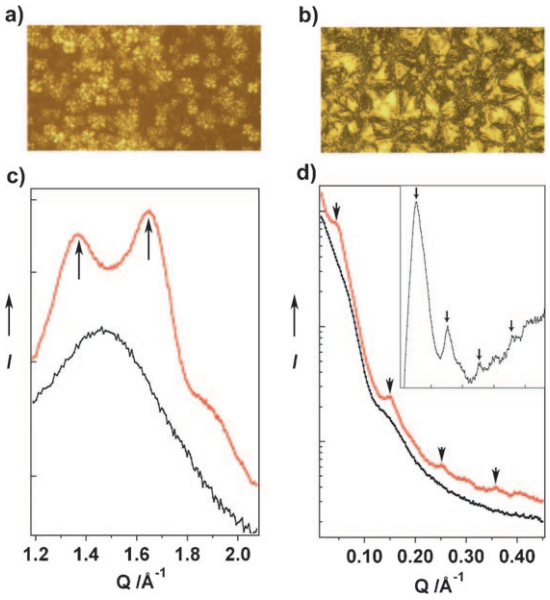

Figure 3. Polarized-light microscopy images showing birefringence from a [**C**-Fn][**S**] melt at 32 °C. The sample was annealed at a) 10 °C min^{-1} and b) 2 °C min^{-1}. c) WAXS profiles from the [**C**-Fn][**S**] melt at 32 °C (red line) 50 °C (black line); arrows indicate Bragg peaks. d) SAXS profiles of a [**C**-Fn][**S**] melt at 50 °C (black line) and at 32 °C (red line). Lamellar reflections are denoted by arrows. Inset: Lorentz-corrected SAXS profile and position of Bragg peaks.

was consistent with ordering of the protein melt into a thermotropic liquid-crystalline phase with smectic microstructure. Larger Maltese cross patterns were observed when the annealing rate was reduced to 2 °C min^{-1} (Figure 3b), indicating that the domain size of the protein liquid crystals depended on the thermal history of the sample. The birefringence persisted until 37 °C, confirming that the second endothermic transition observed in the DSC experiments (arrow in Figure 2a) was associated specifically with loss of the liquid-crystalline phase.

Structural elucidation of the thermotropic liquid-crystalline phase of the [**C**-Fn][**S**] melt was undertaken by wide-angle X-ray scattering (WAXS) and small-angle X-ray scattering (SAXS) measurements recorded over a temperature range of 25 to 50 °C on samples previously annealed at 10 °C min^{-1}. The WAXS profile of [**C**-Fn][**S**] at 32 °C showed two peaks at Q-values of 1.37, 1.65 Å^{-1} (Figure 3c). These values corresponded to repeat distances of 4.6 and 3.8 Å, respectively, and were typical of alkyl tail–tail[10] and polyethylene glycol (PEG) chain–chain interactions.[11] These peaks persisted up to a temperature of about 40 °C, indicating that they were associated specifically with the liquid-crystalline order of the protein fluid. No evidence for short-range order was observed above this temperature; instead the WAXS patterns exhibited a single broad peak at Q = 1.5 Å^{-1} (Figure 3c). This broad peak was also observed in WAXS profiles of the anionic polymer surfactant **S** recorded between temperatures of 25 to 50 °C. Corresponding SAXS profiles for [**C**-Fn][**S**] at 32 and 40 °C showed the presence and absence of long-range order, respectively (Figure 3d). The Bragg reflections observed at 32 °C were in agreement with a lamellar mesophase with a (001) repeat distance of approximately 13 nm, similar to the external diameter of the ferritin molecule (d = 12.5 nm). In addition, whilst the (001) and (003) reflections were relatively intense, those for (002) and (004) were weak, which was consistent with the low-high-low electron-density cross-sectional distribution of a core–shell nano-construct. In contrast, SAXS profiles for the [**C**-Fn][**S**] melt at 50 °C showed no evidence of mesostructural order; instead a small fringe at Q = 0.14 Å^{-1} associated with sphere scattering from the iron oxide cores with a radius of 4 nm was observed (Supporting Information, Figure S5). Control experiments on **S** alone, gave SAXS profiles comprising distinct Bragg peaks that persisted across the temperature range investigated (Supporting Information, Figure S6). The reflections were consistent with a predominately lamellar phase (q1:q2:q3:q4:q5 = 1:2:3:4:5) with lattice parameter value of d = 7 nm.

The above results indicated that the onset of protein fluidity is a direct consequence of the modified surface properties of the [**C**-Fn][**S**] construct, which increase the range of the intermolecular force field to a length scale that is commensurate with the size of the protein molecules, thereby enabling thermally induced molecular motions to be correlated over extended distances. We note that this phenomenon is fundamentally different from that of biphasic systems, which typically consist of a blend of nanoparticles dispersed within a continuous polymer phase that serves as a lubrication medium.[6] Moreover, our results demonstrate the unprecedented formation of a thermotropic liquid-crystalline protein with mesolamellar structure, viscoelasticity, and a stability range between 30 and 37 °C. Formation of the smectic phase is correlated with short-range ordering of the nonylphenyl tails of the surface-attached sulfonated polyethylene oxide polymer, and long-range stacking of layers spaced at a distance commensurate with the molecular diameter of ferritin. This situation is consistent with a structural model involving the stacking of mono-molecular layers of [**C**-Fn][**S**] conjugates in which the in-plane liquidlike arrangement comprises interactions that are stronger than those between adjacent lamellae (Figure 4). The anisotropic ordering appears to be relatively weak as it appears only after melting of the polyethylene oxide chains and is readily overcome by a small increase in temperature.

Although the origin of this anisotropy from a spherically shaped protein is to be determined, we note that the distribution of H- and L-chain subunits within the quaternary structure of ferritin is heterogeneous[12] (Supporting Information, Figure S7), with the consequence that cationization and subsequent conjugation of the polymer surfactant could result in the transformation of the spherical native protein into an ellipsoidal conjugate with an asymmetric distribution of surface functionalities. In support of this mechanism, preliminary AFM measurements on individual [**C**-Fn][**S**] nano-

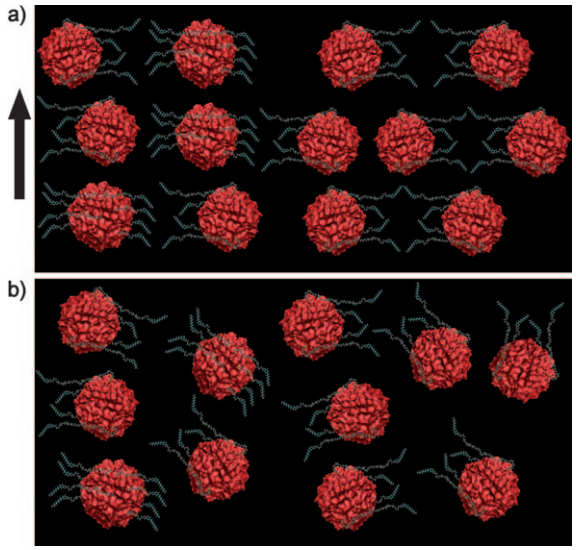

Figure 4. a) Proposed structure of the [**C**-Fn][**S**] melt at 32 °C showing a lamella liquid-crystalline phase viewed side-on to the layer stacking direction (black arrow; **C**-Fn red, **S** green), with a liquidlike in-plane arrangement comprising short-range local ordering interactions between adjacent polymer chains. b) Corresponding Newtonian liquid phase at 50 °C.

constructs showed a small but reproducible deviation from spherical symmetry with an average particle aspect ratio of 1:1.4 (Supporting Information, Figure S8).

Finally, we expect the strategies described herein to contribute significantly to the general preparation of a new class of substances in the form of solvent-free protein melts with zero vapor pressure. We have undertaken similar investigations with cationized apoferritin, as well as native ferritin and apoferritin. Although variations were observed in both the optical and calorimetric responses, the versatility of the method was illustrated by the formation of melts in all instances (Supporting Information, Figure S3, S9, S10). Moreover, as a wide range of biomimetic ferritins with cores reconstituted with metals (Ag,[13] In[14]), quantum dots (CdSe,[15] PbS[16]), magnetic alloys (CoPt),[17] or hydrogenation catalysts (Pd)[18] have been recently prepared and investigated in potential applications,[19] the range of functionalities associated with solvent-free ferritin melts could be readily extended by using synthetically designed ferritins. Our studies indicate that melts of the proteins, myoglobin and lysozyme, can also be prepared[20], suggesting that the method described could be readily developed for a wide range of biologically derived nano-objects and nanostructures.

Experimental Section

Equine spleen ferritin was purchased from Sigma–Aldrich (*F4503*) and dialyzed (Spectra/Por Float-A-Lyzer; 100 kDa MWCO) extensively against Milli-Q quality water containing 50 ppm sodium azide. Demineralization of ferritin to produce apoferritin was achieved by following established procedures.[21,22] Protein concentrations were determined using a Lambda 25 Perkin–Elmer UV-Vis spectrometer and a Sigma–Aldrich Bicinchoninic Acid Kit (*BCA1*). *N*,*N*-dimethyl-1,3-propanediamine (DMPA; *308110*), *N*-(3-*d*imethylaminopropyl)-*N*′-ethylcarbodiimide hydrochloride (EDC; *E1769*), and the surfactant poly(ethylene glycol) 4-nonylphenyl-3-sulfopropyl ether (C_9H_{19}-C_6H_4-$(OCH_2CH_2)_{20}O(CH_2)_3SO_3^-K^+$; **S** = $[C_9PhE_{20}OPrSO_3]^-$; M_r = 1250; *473197*), were used as supplied by Sigma–Aldrich.

Protein cationization: Conjugation of *N*,*N*-dimethyl-1,3-propanediamine (DMPA) to aspartic and glutamic acid residues on the external surface of ferritin or apoferritin was undertaken using carbodiimide activation.[23] Briefly, solutions of DMPA were adjusted to pH 6 using 6 M HCl, and added dropwise to a stirred solution of ferritin or apoferritin. The coupling reaction was initiated by adding *N*-(3-*d*imethylaminopropyl)-*N*′-ethylcarbodiimide hydrochloride (EDC) immediately and again after 5 h. The pH value was maintained using dilute HCl, and solutions were stirred for a further 6 h. The solutions were then centrifuged to remove any precipitate and the supernatant dialyzed (Visking dialysis tubing 12–14 kDa MWCO) extensively against Milli-Q quality water to produce stable solutions of DMPA cationized ferritin ([**C**-Fn]) or apoferritin ([**C**-apoFn]).

Cationization efficiencies were quantitatively assessed using nanospray ionization mass spectroscopy. Samples were introduced as water: acetonitrile : formic acid (500:500:2) solutions at 40 $\mu L\,min^{-1}$ with a gas pressure of 0.3 psi and voltage of 1.4 kV. Native ferritin and apoferritin were run as blanks and the instrument settings were retained for the subsequent cationized protein measurements. Spectra were deconvoluted where possible. Protein/DMPA polycationic conjugates were also studied using analytical ultracentrifugation (AUC) at 25 °C using an Optima XL-I (Beckman-Coulter). Sedimentation velocity experiments were performed in 0.1 M NaCl solution on the native and cationized proteins with $c <$ 1.2 $mg\,mL^{-1}$ (ferritin) and 3.1 $mg\,mL^{-1}$ (apoferritin) at 5000 and 20000 rpm (apoferritin) and 10000 rpm (ferritin) followed by 60000 rpm to check for non-coordinated small molecules and the sedimentation coefficient (s) used to estimate the nature of the protein–protein and protein–DMPA interactions.

Protein melts: 5 $mg\,mL^{-1}$ of an aqueous solution of cationized ferritin ([**C**-Fn]) was added to a stirred viscous liquid of **S** to give a ferritin:surfactant ratio of 1:3 w/w. The solution was stirred for 12 h, centrifuged to remove any precipitate, and the supernatant dialyzed (Visking dialysis tubing 12–14 kDa MWCO) extensively against Milli-Q quality water. The dispersed protein–surfactant nanostructures were investigated by TEM and AUC to determine the structural integrity and stoichiometry of the [**C**-Fn][**S**] ionic constructs in aqueous solution. Aqueous samples of [**C**-Fn][**S**] were lyophilized for 48 h and the resulting nanostructured ionic solids stored in a desiccator under vacuum. Protein melts were prepared by annealing the lyophilized/desiccated [**C**-Fn][**S**] solids at 50 °C to produce clear viscous red liquids that remained fluid when cooled to room temperature.

Ionic nanostructures and corresponding melts prepared from [**C**-Fn][**S**] were studied using a range of techniques. In each case, care was taken to control the thermal history of the samples. The decomposition temperature and residual water content of the ionic constructs were determined by thermogravimetric analysis (TGA). Differential scanning calorimetry (DSC) was used to map the enthalpic phase transitions between −50 and 60 °C. Samples were heated/cooled at a rate of 10 °C $minute^{-1}$ and isothermal cycles repeated to examine the level of reversibility and thermal hysteresis. Rheometry was used to establish the liquidlike behavior and probe the temperature-dependent viscoelastic properties of the protein melts. Annealed samples were investigated under oscillating (frequency sweeps) and static conditions (viscometry) at temperatures between (32 °C) and above (50 °C) the endothermic transitions shown from DSC studies. A Bohlin CVO rheometer with a 10 mm parallel plate geometry was used throughout.

Polarized-light microscopy (PLM) was performed using the same temperature program as employed in the DSC experiments, to correlate the enthalpic transitions with changes in optical properties and liquid-crystalline behavior. Wide- and small-angle X-ray scattering (WAXS and SAXS) were used to probe the structural origins of

the temperature–dependent optical properties at sub-nanometer resolution. Experiments were undertaken on previously annealed samples at temperatures above and below the thermal transitions determined by DSC. Samples for scattering experiments were mounted in either biaxially-oriented polyethylene terephthalate (boPET) (WAXS) or mica (SAXS) cells. Samples for TEM were prepared on carbon-coated copper grids either by dissolving the melt in water, or by applying the melt directly to the grid followed by in situ annealing.

Similar preparations and experiments as described above were undertaken using native ferritin, native apoferritin, or [**C**-apoFn] in place of [**C**-Fn].

Received: June 9, 2009
Published online: July 14, 2009

Keywords: liquid crystals · melts · nanostructures · proteins · viscoelasticity

[1] C. M. Niemeyer, C. A. Mirkin, *Nanobiotechnology: Concepts, Applications and Perspectives*, *Illustrated ed.*, Wiley-VCH, Weinheim, **2004**.
[2] E. Katz, I. Willner, *Angew. Chem.* **2004**, *116*, 6166 – 6235; *Angew. Chem. Int. Ed.* **2004**, *43*, 6042 – 6108.
[3] C. M. Niemeyer, *Angew. Chem.* **2001**, *113*, 4254 – 4287; *Angew. Chem. Int. Ed.* **2001**, *40*, 4128 – 4158.
[4] E. V. Shevchenko, D. V. Talapin, N. A. Kotov, S. O'Brien, C. B. Murray, *Nature* **2006**, *439*, 55 – 59.
[5] S. C. Warren, M. J. Banholzer, L. S. Slaughter, E. P. Giannelis, F. J. DiSalvo, U. B. Wiesner, *J. Am. Chem. Soc.* **2006**, *128*, 12074 – 12075.
[6] R. Rodriguez, R. Herrera, L. A. Archer, E. P. Giannelis, *Adv. Mater.* **2008**, *20*, 4353 – 4358.
[7] A. B. Bourlinos, R. Herrera, N. Chalkias, D. D. Jiang, Q. Zhang, L. A. Archer, E. P. Giannelis, *Adv. Mater.* **2005**, *17*, 234 – 237.
[8] A. B. Bourlinos, S. R. Chowdhury, R. Herrera, D. D. Jiang, Q. Zhang, L. A. Archer, E. P. Giannelis, *Adv. Funct. Mater.* **2005**, *15*, 1285 – 1290.
[9] Y. J. Min, M. Akbulut, K. Kristiansen, Y. Golan, J. Israelachvili, *Nat. Mater.* **2008**, *7*, 527 – 538.
[10] E. A. Ponomarenko, A. J. Waddon, K. N. Bakeev, D. A. Tirrell, W. J. MacKnight, *Macromolecules* **1996**, *29*, 4340 – 4345.
[11] H. Lee, R. M. Venable, A. D. MacKerell, R. W. Pastor, *Biophys. J.* **2008**, *95*, 1590 – 1599.
[12] P. M. Harrison, P. Arosio, *Biochim. Biophys. Acta Bioenerg.* **1996**, 1275, 161 – 203.
[13] R. M. Kramer, C. Li, D. C. Carter, M. O. Stone, R. R. Naik, *J. Am. Chem. Soc.* **2004**, *126*, 13282 – 13286.
[14] M. Okuda, Y. Kobayashi, K. Suzuki, K. Sonoda, T. Kondoh, A. Wagawa, A. Kondo, H. Yoshimura, *Nano Lett.* **2005**, *5*, 991 – 993.
[15] I. Yamashita, J. Hayashi, M. Hara, *Chem. Lett.* **2004**, *33*, 1158 – 1159.
[16] B. Hennequin, L. Turyanska, T. Ben, A. M. Beltran, S. I. Molina, M. Li, S. Mann, A. Patane, N. R. Thomas, *Adv. Mater.* **2008**, *20*, 3592.
[17] B. Warne, O. I. Kasyutich, E. L. Mayes, J. A. L. Wiggins, K. K. W. Wong in *International Magnetics Conference (INTERMAG 2000)*, Ieee-Inst Electrical Electronics Engineers Inc, Toronto, Canada, **2000**, pp. 3009–3011.
[18] T. Ueno, M. Suzuki, T. Goto, T. Matsumoto, K. Nagayama, Y. Watanabe, *Angew. Chem.* **2004**, *116*, 2581 – 2584; *Angew. Chem. Int. Ed.* **2004**, *43*, 2527 – 2530.
[19] I. Yamashita, *J. Mater. Chem.* **2008**, *18*, 3813 – 3820.
[20] A. W. Perriman, S. Mann, unpublished results.
[21] A. Treffry, P. M. Harrison, *Biochem. J.* **1978**, *171*, 313 – 320.
[22] F. Funk, J. P. Lenders, R. R. Crichton, W. Schneider, *Eur. J. Biochem.* **1985**, *152*, 167 – 172.
[23] D. Danon, E. Skutelsk, Y. Marikovs, L. Goldstei, *J. Ultrastruct. Res.* **1972**, *38*, 500 – 510.

